

Comparing grain size and dislocation density effects for hysteresis loops with the same maximum flux density in a magnetic hysteresis model

M. J. Sablik

Southwest Research Institute, P.O. Drawer 28510, San Antonio, Texas 78228-0510

F. J. G. Landgraf

Institute for Technological Research, IPT, Av. Prof. Almeida Prado 532, CEP5508-901, Sao Paulo, Brazil

ABSTRACT

Microstructural attributes such as grain size and dislocation density affect the hysteretic magnetic properties of steels because microstructure affects domain wall movement and pinning. The consensus experimentally is that both coercivity and hysteresis loss tend to be linearly related to the inverse of the average grain diameter and to the square root of the dislocation density (viz. $\zeta_d^{1/2}$). In an earlier paper, a model was proposed for computing hysteresis loops based on the effect of grain size and dislocation density. In that paper, hysteresis loops were compared that all had the same maximum field H_{max} . The result was that coercivity departed from the linear relationships with inverse grain size (viz. $1/d$) and $\zeta_d^{1/2}$ for large values of $1/d$ and $\zeta_d^{1/2}$. The same was true of hysteresis loss W_H , except that hysteresis loss even showed a peak, first increasing and then decreasing with increasing $1/d$ and $\zeta_d^{1/2}$. This kind of behavior had not been seen by experimenters, particularly core loss people. It was learned, however, that the core loss experimenters compared hysteresis loops of the same maximum flux density B_{max} instead of the same H_{max} . In this paper, therefore, we use the model previously formulated to produce hysteresis loops with the same B_{max} . Indeed, the appropriate linear relationships are found. The paper also addresses effects of uniaxial anisotropy on microstructural magnetic effects.

PACS nos. 81.40.Rs, 75.60.Ej, 75.60.-d, 81.70.Ex

I. INTRODUCTION

In steel, microstructure influences magnetic properties because it has an important effect on the density of domain walls and on the pinning and unpinning of domain walls. These domain wall attributes ultimately are responsible for the hysteretic behavior of magnetic properties.

Two important features of the microstructure that affect magnetic hysteresis are (1) grain size (i.e., average grain diameter d) and (2) dislocation density ζ_d . As grain size decreases, the total length of grain boundary increases. Since the grain boundary is often associated with the pinning of domain walls, it follows that with decreasing grain size, the pinning of domain wall motion increases. Since coercivity H_c reflects amount and strength of pinning, we expect H_c to increase as d decreases. Similarly, as dislocation density increases, dislocations begin to get entangled, forming strong pinning centers for domain walls, so impeding domain wall motion. Thus, as ζ_d increases, so also does H_c . It has been generally established experimentally¹⁻⁴ that H_c has a linear relationship with respect to $A + B/d$ and $\zeta_d^{1/2}$, where A and B are constants. A similar relationship was also generally to be found for hysteresis loss W_H .^{5,6}

Despite all this experimental work, no one had actively pursued the question of modeling the effect of grain size and dislocation density on magnetic hysteresis. In two recent papers,^{7,8} this changed when one of the present authors (M.S.) presented a hysteresis model which was a modification of an earlier hysteresis model due to Jiles and Atherton.⁹ The model successfully exhibited the linear behavior with $A + B/d$ and $\zeta_d^{1/2}$ for grain sizes of the order of larger than 15μ (where μ represents 1 micron = 10^{-6} m) and dislocation densities of the order of $5 \times 10^{10}/\text{m}^2$ or less. In comparing between hysteresis loops for different grain sizes and dislocation densities, the loops were all taken to the same maximum magnetic field H_{max} . The result appeared to agree with experimental results, since all the published experiments were restricted to grain sizes somewhat larger than 15μ . Core loss experimenters, however, have privately indicated that they

have found linear results for smaller grain sizes than 15μ . However, they compare hysteresis loops taken to a constant B_{max} instead of a constant H_{max} .

It was decided therefore, in this paper, to compare modeled hysteresis loops, all taken to the same B_{max} . It was reasoned that for constant B_{max} , the remanence B_r would remain approximately constant regardless of grain size and dislocation density. Thus, hysteresis loss W_H , which is approximately $B_r H_c$, should show the same pattern of behavior as H_c . On the other hand, in the case where all the loops are taken to a constant H_{max} , the remanence decreases with increasing inverse grain size and dislocation density, whereas the coercivity increases, causing a competition between B_r and H_c in contribution to W_H , with a maximum resulting in W_H due to the competition. We thus expect much more regular behavior in the dependence of H_c and W_H on grain size and dislocation density for loops of constant B_{max} . We find this and some other interesting phenomena as well.

II. THE MODEL

We start by referring to the basic hysteresis model of Jiles and Atherton,⁹ which has been modified to include the effect of stress by Sablik and Jiles.¹⁰

In the Jiles-Atherton model, the total magnetization M is the sum of a reversible (M_{rev}) and an irreversible (M_{irr}) component. These components are given by

$$M_{rev} = c (M_a - M_{irr}) \quad (1)$$

$$M_{irr} = M_a - \frac{k}{\mu_0} \frac{\delta}{dH_e} \frac{dM_{irr}}{dH_e} \quad (2)$$

Here, M_a is the anhysteretic magnetization, given as

$$M_a(H_e) = M_s L(H_e/a), \quad (3)$$

where the function $L(x) = \coth x - 1/x$ is the so-called Langevin function, and where H_e is the effective magnetic field inside the material, i.e.

$$H_e = H + \alpha M_a . \quad (4)$$

The five parameters M_s , c , a , k , and α are all parameters of the material. The number δ , taking the value +1 or -1, depending on whether H is increasing or decreasing, corresponds mathematically with the hysteresis. Eq. (2) is actually a differential equation. A more transparent form of Eq. (2) is given by^{9,10}

$$dM_{irr}/dH = (M_a - M_{irr}) / [(k\delta/\mu_o) + \alpha(M_a - M_{irr})] . \quad (5)$$

We expect that microstructure will affect all five material parameters cited above, although some more than others. In particular, grain size and dislocation density have important effects on the domain wall pinning parameter k and the effective field scaling parameter a , which is a function of the domain density.

Since the domain wall pinning constant k mathematically controls the amount of hysteresis that is present, it is proportional to the coercivity and hence must have the same dependences as exhibited by the coercivity. Thus, we write that

$$k = [G_1 + G_2/d] \zeta_d^{1/2} k_o . \quad (6)$$

We define the constant G_1 and G_2 as follows. For the specific values of $d = d^* = 20\mu$ and $\zeta_d = \zeta_d^* = 1 \times 10^{12} / \text{m}^2$, we choose G_1 and G_2 so that

$$(G_1 + G_2/d^*) (\zeta_d^*)^{1/2} = 1 . \quad (7)$$

A choice that satisfies this is $G_2 = 10 \times 10^{-12} \text{ m}^2$ and $G_1 = 0.5 \times 10^{-6} \text{ m}$. As we shall see below, there are other choices for G_2 and G_1 that satisfy Eq. (7). We shall explore some of these below, and we shall find that the different choices determine the amount of spread in the hysteresis

behavior due to variation of grain size and dislocation density. Note that when d and ζ_d satisfy Eq. (7) (i.e., when $d = d^*$ and $\zeta_d = \zeta_d^*$), then $k = k_o$. The 20μ choice for grain size d^* represents a typical grain size that has been investigated. The choice of $\zeta_d^* = 1 \times 10^{12}/m^2$ represents a dislocation density quoted by papers on plastic deformation as a typical value for dislocation density in undeformed steel.^{4,6,11,12} It should be pointed out however that other papers^{1,13} have quoted values of the order $10^{10}/m^2$, and such values were used in Refs. [7] and [8]. Because the range of dislocation density here is now of order $10^{12}/m^2$, the values of G_1 and G_2 are changed to accommodate the new range of dislocation density.

The effective field scaling constant a is proportional to the domain density in the demagnetized state.¹⁰ This domain density will be determined by the pinning site density, which in turn is proportional^{9,10} to the pinning constant k . It follows, therefore, that the scaling constant a should have the same dependence on d and ζ_d that k has, and hence we have that

$$a = \{[G_3 + G_4/d]\zeta_d^{1/2}\}a_o. \quad (8)$$

If we define G_3 and G_4 in the same way as G_1 and G_2 , using Eq. (7) for $d = d^*$ and $\zeta_d = \zeta_d^*$, then we can choose $G_3 = G_1$ and $G_4 = G_2$.

Eqs. (6)–(8) represent the microstructural modification that has been made to the Jiles-Atherton model. Later, as we explore the numerical results, we shall discover some additional consequences of the above model.

III. RESULTS

In the following analysis, we have restricted the values of grain size d to 10μ , 15μ , 20μ , 25μ , and 30μ . Also, we have restricted the values of dislocation density ζ_d to 0.25, 0.49, 1, 2.25 and $4 \times 10^{12}/m^2$. Thus, we look at a matrix of 25 different conditions for the microstructure. The two most extreme conditions occur for microstructural value sets of $(4 \times 10^{12}/m^2, 10\mu)$ and

$(0.25 \times 10^{12} /m^2, 30\mu)$. For hysteresis loops all of the same B_{max} , the former value set corresponds to the loop with largest H_{max} , and the latter value set corresponds to the loop with smallest H_{max} .

Figure 1 shows hysteresis loops corresponding to (a) the former value set for (ζ_d, d) with $B_{max} = 1.03$ T and (b) the latter value set, again with $B_{max} = 1.03$ T. By keeping B_{max} constant for all the hysteresis loops, we end up with loops of widely varying shape, as we vary d and ζ_d . For the loops here, we have taken $c = 0.25$, $k_0/\mu_0 = 1200$ A/m (where μ_0 is the permeability of free space), $a_0 = 1100$ A/m, $\alpha = 8.44 \times 10^{-6}$ (where α is related to λ_s via Eq. (30) in Ref. [10]), and $M_s = 1.585 \times 10^6$ A/m. Also, we have used the values for G_2 and G_1 given just below Eq. (7).

Figure 2 is for the choice $G_2 = 3.8 \times 10^{-12} m^2$ and $G_1 = 0.81 \times 10^{-6} m$. One may check that Eq. (7) is still satisfied for $d = d^* = 20\mu$ and $\zeta_d = \zeta_d^* = 1 \times 10^{12}/m^2$ with these choices of G_1 and G_2 . For this choice of parameters, and with $k_0/\mu_0 = 1000$ A/m, $a_0 = 900$ A/m, $c = 0.25$ and $M_s = 1.585 \times 10^6$ A/m, we can choose $B_{max} = 1.40$ T and are still able to have all the loops with the same B_{max} . Notice that the loops shown in Fig. 1 not only differ in H_{max} , but also their shapes indicate that both are far from saturation. The loops in Fig. 2 also are still far from saturation. We can get these loops closer to saturation by choosing k_0 , a_0 , and c differently.

Figure 3 is for the choice $k_0/\mu_0 = 500$ A/m, $a_0 = 600$ A/m, $c = 0.25$, and $M_s = 1.585 \times 10^6$ A/m, with α the same as in Figs. 1 and 2 and with G_1 and G_2 the same as in Fig. 2. We compare loops this time with $B_{max} = 1.66$ T. These loops are closer to saturation, but we can still do better.

In Fig. 4, the parameter choice is $k_0/\mu_0 = 100$ A/m, $a_0 = 100$ A/m, $c = 0.25$, and $M_s = 1.585 \times 10^6$ A/m, with α remaining the same and with G_1 and G_2 as in Fig. 2. This choice leads to loops with $B_{max} = 1.94$ T, which are close to saturation, as seen from the shapes in Fig. 4. The loops obviously correspond to rather soft materials, compared to those seen in Fig. 1.

We now compare the magnetic properties of coercive field H_c , relative permeability μ/μ_0 at field $H = H_c$, remanent flux density B_r , and hysteresis loss W_H for all the various loops in each set of 25 loops corresponding to the different (ζ_d, d) .

Figure 5 is a set of plots of the different magnetic properties against the square root of the dislocation density. The various material parameters are set as in Fig. 1. Two things are striking about this figure. The coercive field H_c is directly proportional to the square root of the dislocation density for all values of $\zeta_d^{1/2}$, exhibiting different slopes for different grain sizes. There is no deviation from linear proportionality, as is seen for the curves when loops of the same H_{max} are compared. (See Ref. [7] for curves corresponding to such loops.) Thus, it would appear that the better way to compare hysteresis loops for different grain sizes and dislocation density is to compare loops that are all taken to the same B_{max} . The same is true for hysteresis loss W_H . The hysteresis loss is also seen to be directly proportional to the square root of the dislocation density in this model for all values of $\zeta_d^{1/2}$, again exhibiting different slopes for different grain sizes. There is no maximum in W_H , as was found when loops of the same H_{max} were compared.⁷ The relative permeability at H_c does not exhibit linear behavior and decreases nonlinearly with increasing $\zeta_d^{1/2}$. This is similar to what was observed⁷ for loops all with the same H_{max} . The remanent flux density B_r is approximately the same for all values of ζ_d and d , as was anticipated. (See the Introduction.)

In Fig. 6, we again see plots of magnetic properties against the square root of the dislocation density, but this time parameters are chosen as in Fig. 2. Qualitatively, the variations are similar to Fig. 5. One new attribute is that now the choice of G_1 and G_2 causes all the plots for the different grain sizes to be less spread apart. The linear proportionality is again observed for H_c and W_H as plotted against $\zeta_d^{1/2}$. Relative permeability at H_c again behaves nonlinearly and

decreases with increasing $\zeta_d^{1/2}$. Again, B_r is approximately constant, as anticipated, although showing a very slight decrease with increasing $\zeta_d^{1/2}$.

In the case of Fig. 7, the parameters are the same as in Fig. 3. Qualitatively, the behavior is similar to Fig. 6, except that H_c and W_H values are smaller, and relative permeability at H_c is larger.

Figure 8 is for the case where the parameters are the same as in Fig. 4. In this case, the parameters are set so as to produce a rather soft material. Qualitatively, the parameters behave much the same as in Figs. 6 and 7, with some important exceptions. The coercive field values are a lot smaller. The relative permeability values at H_c are a lot larger. The W_H values are a lot smaller. Furthermore, an instability is beginning to show up in W_H , and we only see a trend toward linear proportionality with $\zeta_d^{1/2}$ but not a true linear proportionality. This is presumably due to two things. The numerical error in evaluating the hysteresis loss is getting larger, percentagewise. The model is also nearing an instability because, after all, it is alternatively called the “domain wall pinning model” and is not meant for truly soft materials.

We also look at plots of the magnetic properties against inverse grain size.

Figure 9 shows such plots for the material parameters chosen for Figs. 1 and 5. Again, we return to large values of H_c and W_H , and smaller values for the relative permeability at H_c . It is seen that the H_c and W_H vary essentially linearly with inverse grain sizes, but with plots for different dislocation densities ζ_d having different intercepts. The relative permeability at H_c varies nonlinearly, decreasing with increasing inverse grain size $1/d$. The remanent flux density is approximately constant for the various grain sizes and dislocation densities.

In Fig. 10, the material parameters are chosen as in Figs. 2 and 6. Except for change in range of values of the magnetic properties, the functional dependences are as they were in Fig. 9.

Figure 11, for parameters as in Figs. 3 and 7, also shows similar functional dependences.

Figure 12 is for material parameters chosen as in Figs. 4 and 8. This is for the soft material. Notice that the H_c and W_H values are again considerably smaller and the relative permeability at H_c is considerably larger. The linear behaviors seen in Fig. 7 are again seen here, except that deviations from linearity occur for W_H at the smaller dislocation densities. Again, this is due both to numerical error in integration and to the approach of an instability in the model in the case of very soft materials, possibly due to numerical error in solving the differential Eq. (5) numerically.

IV. INCLUSION OF UNIAXIAL ANISOTROPY

It is possible to modify the basic model, as outlined in Eqs. (1)–(5), so as to include the effects of uniaxial anisotropy. According to Ref. [14], Eqs. (1)–(5) become modified as follows.

The key modification is that the effective field H_e is now

$$H_e = H + (\alpha - \kappa_u) M_a, \quad (9)$$

where

$$\kappa_u = 2 K_u / (\mu_0 M_s^2), \quad (10)$$

where K_u is a measure of the uniaxial anisotropy energy E_u per unit volume. This all means that Eq. (3) for M_a is now changed because of the dependence of M_a on H_e . Similarly, Eq. (5) for dM_{irr}/dH changes explicitly with the explicit replacement of α by $\alpha - \kappa_u$. The total magnetization $M = M_{irr} + M_{rev}$, and, as above, Eq. (1) is used to obtain M_{rev} .

In this section, we study the effects of uniaxial anisotropy, due perhaps to grain orientation, on the magnetic hysteresis properties. For this case, $M_s = 1.585 \times 10^6$ A/m, $k_0/\mu_0 = 500$ A/m, $a_0 = 600$ A/m, $c = 0.25$ and G_1 and G_2 are as in Figs. 2–4, 6–8, and 10–12. We note in particular that the parameter choice corresponds to Figs. 3, 7, and 11. We examine three cases of anisotropy, namely $K_u = -1200$ J/m³, 0, and +1200 J/m³.

The interesting plots are those of magnetic properties against the square root of the dislocation density ζ_d . Figure 13 shows these plots for H_c and W_H . In particular, while the plots of H_c vs. $\zeta_d^{1/2}$ and W_H vs. $\zeta_d^{1/2}$ still exhibit linear behavior, the plots for the different grain sizes extrapolate to a value along the ordinate axis that is nonzero when K_u is nonzero. In particular, when $K_u = +1200 \text{ J/m}^3$ (and with $B_{max}=1.62 \text{ T}$ for the loops), the value to which the H_c and W_H plots extrapolate is positive and nonzero, and so the H_c and W_H cannot ever be zero in this anisotropic case. On the other hand, when $K_u = -1200 \text{ J/m}^3$ (and with $B_{max}=1.70 \text{ T}$ for the loops), the intercept to which H_c and W_H extrapolate is negative, which actually cannot be a physical value because H_c and W_H can only be positive. The extrapolated lines also intercept the abscissa axis. All values of the abscissa $\zeta_d^{1/2}$ less than the extrapolated value at the abscissa intercept are values in this case for which the hysteresis model is unstable and for which it cannot be used. Thus, with anisotropy included, the hysteresis model points to physical limitations in some instances.

To see why the ordinate intercept is nonzero when K_u is nonzero, remember that the Langevin function $L(x) = \coth(x) - 1/x$, and recall that the series for $\coth(x)$ is such that

$$L(x) \approx x/3 - x^3/45 + 2x^5/945 \approx x/3, \quad (11)$$

and since $x = H_e/a$, we have that

$$M_a/M_s \approx [H + (\alpha - \kappa_u) M_a]/3a. \quad (12)$$

If $H=H_c$, then from Eq. (12), it follows that

$$H_c \approx 3aM_a(H_c)/M_s - (\alpha - \kappa_u)M_a(H_c) \quad (13)$$

If K_u is negative, the anisotropy term $\kappa_u M_a(H_c)$ subtracts from the $K_u = 0$ value of H_c . If $K_u > 0$, it adds. Also note that if pinning constant k_0 tends to zero, then M tends to M_a and since $M = 0$ at $H = H_c$, it follows that with $K_u = 0$, then

$$H_c \approx ((3a/M_s) - \alpha)M_a(H_c) \approx ((3a/M_s) - \alpha)M(H_c) = 0. \quad (14)$$

Thus, we see that the H_c intercept is zero when $K_u = 0$, and nonzero otherwise.

If one uses Eq. (8) for a , then

$$H_c \approx \left\{ (3a_0/M_s) [G_1 + G_2/d] \zeta_d^{1/2} - (\alpha - \kappa_u) \right\} M_a(H_c). \quad (15)$$

Thus, consistent with the behavior of the model and experiment, it clearly is seen that H_c is linearly dependent on $\zeta_d^{1/2}$ and on $[G_1 + G_2/d]$. Note that this behavior derives from a , and hence a must behave like k does, as we have asserted earlier, using a different argument.

Finally, it should be pointed out that these arguments depend on the x^3 term being small so that higher order terms in the series in Eq. (11) can be neglected. Fixing H_{max} instead of B_{max} can require the inclusion of these higher order terms because some of the fixed H_{max} hysteresis curves would have to be taken to high values of $x = H_c/a$, and hence one expects deviations similar to those observed in the original paper, Ref. [7].

V. CONCLUSIONS

We conclude that comparing hysteresis plots for different grain sizes and dislocation densities which all have the same B_{max} is quite different from comparing hysteresis plots all with the same H_{max} . The expected linear proportionality of H_c and W_H with $\zeta_d^{1/2}$ and $(G_1 + G_2/d)$ is more evident when comparing hysteresis plots all at the same B_{max} , as is done experimentally.

VI. ACKNOWLEDGMENTS

This project was funded by the U.S. Army Research Office under Contract Number DMD18-99-C-0041.

REFERENCES

1. J. F. Bussiere, *Mater. Eval.* **44**, 560 (1986).
2. B. K. Tanner, J. A. Szpunar, S. N. M. Willcock, L. L. Morgan, and P. A. Mundell, *J. Mater. Sci. Lett.* **24**, 4534 (1988).
3. H. Kronmuller, *Intl. J. Nondestr. Testing* **3**, 315 (1972).
4. J. Sternberk, E. Kratochilova, A. Gemperle, V. Faja, and V. Walder, *Czech. J. Phys. B* **35**, 1259 (1985).
5. G. Ban, P. E. Di Nunzio, S. Cicale, and T. Belgrand, *IEEE Trans. Magn.* **34**, 1174 (1998).
6. J. Sternberk, E. Kratochilova, J. Hrebik, and A. Gemperle, *Phys. Status Solidi A* **79**, 523 (1983)
7. M. J. Sablik, *J. Appl. Phys.* **89**, 5610 (2001).
8. M. J. Sablik, D. Stegemann, and A. Krysz, *J. Appl. Phys.* **89**, 7254 (2001).
9. D. C. Jiles and D. L. Atherton, *J. Magn. Magn. Mater.* **61**, 48 (1986).
10. M. J. Sablik and D. C. Jiles, *IEEE Trans. Magn.* **29**, 2113 (1993).
11. A. S. Keh, *Phil. Mag.* **12**, 9 (1965).
12. E. Lubitz, *J. Appl. Phys.* **4**, 51 (1974)
13. A. H. Qureshi and L. N. Chaudhary, *J. Appl. Phys.* **41**, 1042 (1970)
14. M. J. Sablik, S. W. Rubin, L. A. Riley, D. C. Jiles, D. A. Kaminski, and S. B. Biner, *J. Appl. Phys.* **74**, 480 (1993).

FIGURE CAPTIONS

- Fig. 1.** Hysteresis loops for: (a) $(\zeta_d, d) = (4 \times 10^{12}/m^2, 10\mu)$; (b) $(\zeta_d, d) = (0.25 \times 10^{12}/m^2, 30\mu)$, with $k_0/\mu_0 = 1200$ A/m, $a_0 = 1100$ A/m, $c = 0.25$, and $M_s = 1.585 \times 10^6$ A/m. Also, for this set, $G_2 = 10 \times 10^{-12} m^2$ and $G_1 = 0.5 \times 10^{-6} m$. The rest of the loops for the tested set have H_{max} falling between the depicted two loops. All loops in the set have the same $B_{max} = 1.03$ T.
- Fig. 2.** Hysteresis loops for the same cases of dislocation density and grain size as in Fig. 1, but with $k_0/\mu_0 = 1000$ A/m and $a_0 = 900$ A/m. For this set, $G_2 = 3.8 \times 10^{-12} m^2$ and $G_1 = 0.81 \times 10^{-6} m$. Here, the loops have $B_{max} = 1.40$ T.
- Fig. 3.** Hysteresis loops for the same cases of dislocation density and grain size as in Fig. 1, but now for $k_0/\mu_0 = 500$ A/m and $a_0 = 600$ A/m, and all other parameters the same as in Fig. 2, except that here the loops have $B_{max} = 1.66$ T.
- Fig. 4.** Hysteresis loops for the same cases of dislocation density and grain size as in Fig. 1, but with changes of $k_0/\mu_0 = 100$ A/m and $a_0 = 100$ A/m, and all other parameters as in Fig. 2. Here, the loops have $B_{max} = 1.94$ T.
- Fig. 5.** Magnetic properties against square root of dislocation density, with material parameters set as in Fig. 1. Shown are coercive field H_c , relative permeability μ/μ_0 at H_c , remanent flux density B_r , and hysteresis loss, W_H . The coercive field and hysteresis loss exhibit a direct proportionality to the square root of the dislocation density, $\zeta_d^{1/2}$.
- Fig. 6.** Magnetic properties against $\zeta_d^{1/2}$, with parameters set as in Fig. 2. The straight line plots corresponding to different grain sizes are now closer together than in Fig. 5, in the case of coercive field and hysteresis loss.
- Fig. 7.** Magnetic properties against $\zeta_d^{1/2}$, with parameters as in Fig. 3. Direct proportionalities appear for H_c and W_H vs. $\zeta_d^{1/2}$

- Fig. 8.** Magnetic properties against $\zeta_d^{1/2}$, with parameters as in Fig. 4. Again, direct proportionalities appear for H_c vs. $\zeta_d^{1/2}$, but this time W_H shows signs that the calculation, perhaps due to numerical integration error, is approaching a slight instability and the linear proportionality between W_H and $\zeta_d^{1/2}$ is only approximated.
- Fig. 9.** Plots of magnetic properties against inverse grain size. The plots for each value of dislocation density correspond to straight lines with different intercepts, as inverse grain size is varied in the case of H_c and W_H . Here, parameter values are as in Figs. 1 and 5.
- Fig. 10.** More plots of magnetic properties against inverse grain size, but with parameter values as in Figs. 2 and 6. The straight line plots here have a smaller slope.
- Fig. 11.** Plots of magnetic properties against inverse grain size for the parameter values in Figs. 3 and 7. Again, we see straight line plots similar to Figs. 9 and 10.
- Fig. 12.** Plots of magnetic properties against inverse grain size, but with parameter values as in Figs. 4 and 8. Here the values of H_c and W_H are noticeably smaller. Straight line plots appear for H_c against $1/d$, but for W_H against $1/d$, the lines are only approximately straight.
- Fig. 13.** Plots of (a) coercive field and (b) hysteresis loss against square root of dislocation density for different grain sizes, and for different anisotropies K_u . It is seen that the straight lines for the different anisotropies converge to different intercepts. It is shown in the text how this phenomenon arises mathematically from the model. Here, parameters are set as in Figs. 3, 7, and 11, with $k_0/\mu_0 = 500$ A/m and $a_0 = 600$ A/m.

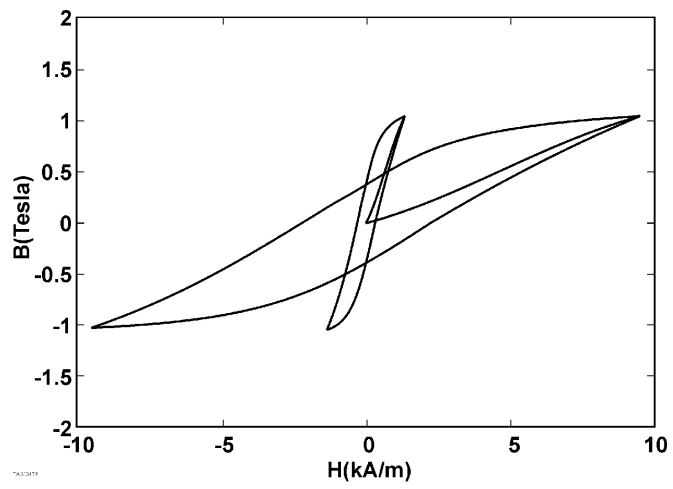


Fig. 1, M. J. Sablik, Journal of Applied Physics

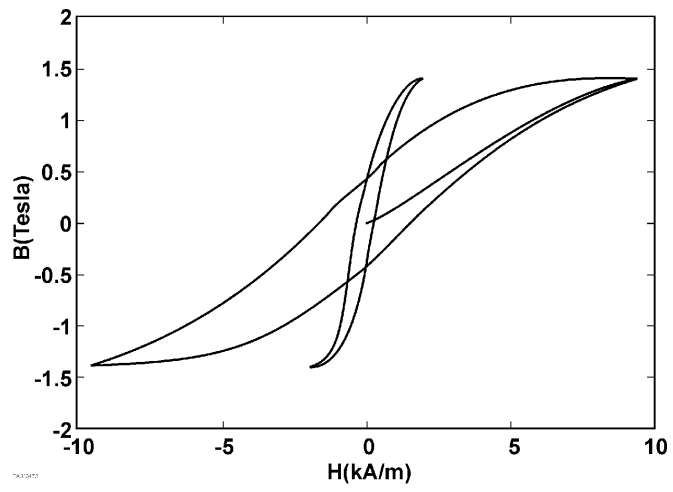


Fig. 2, M. J. Sablik, Journal of Applied Physics

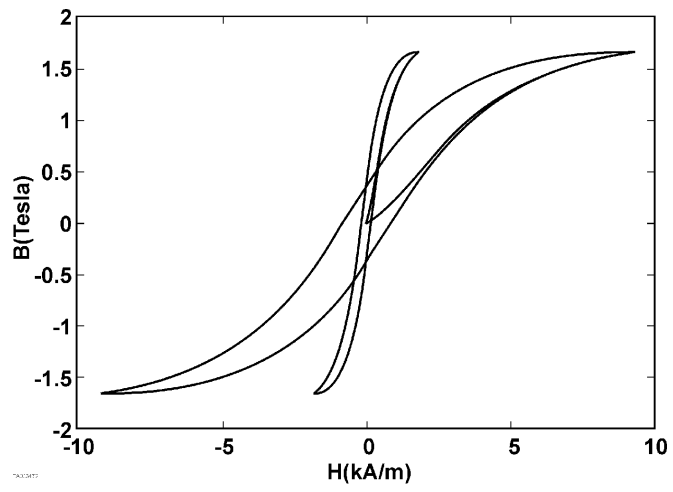


Fig. 3, M. J. Sablik, Journal of Applied Physics

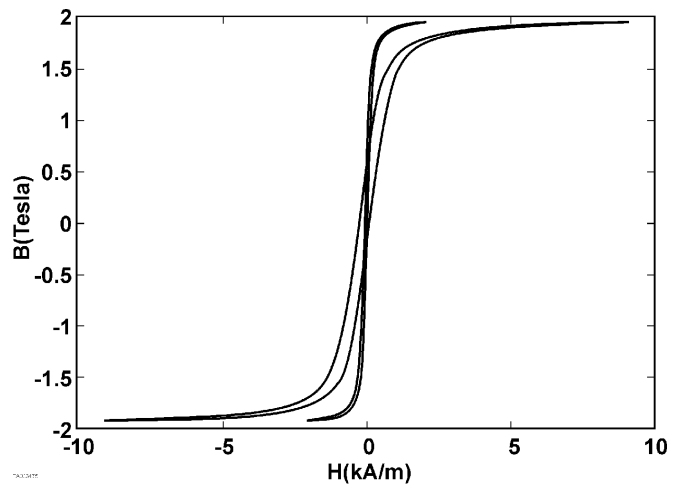


Fig. 4, M. J. Sablik, Journal of Applied Physics

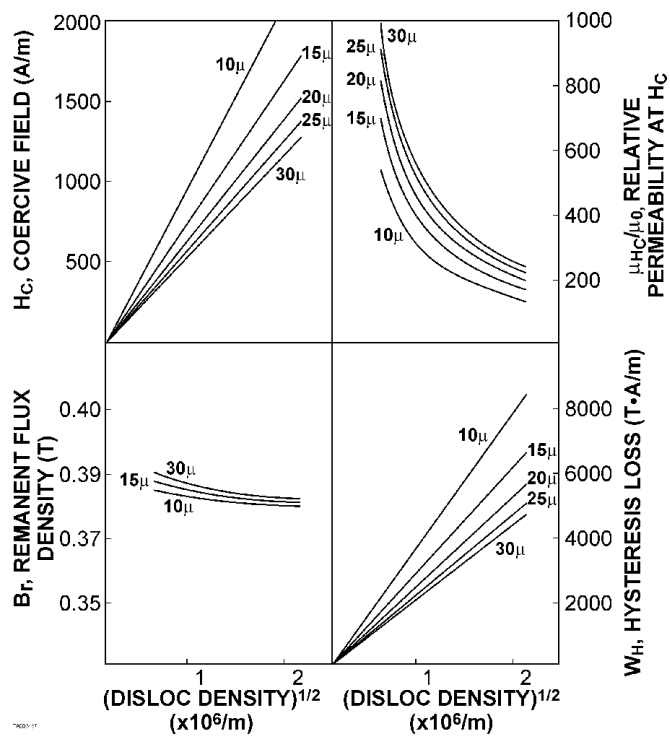


Fig. 5, M. J. Sablik, Journal of Applied Physics

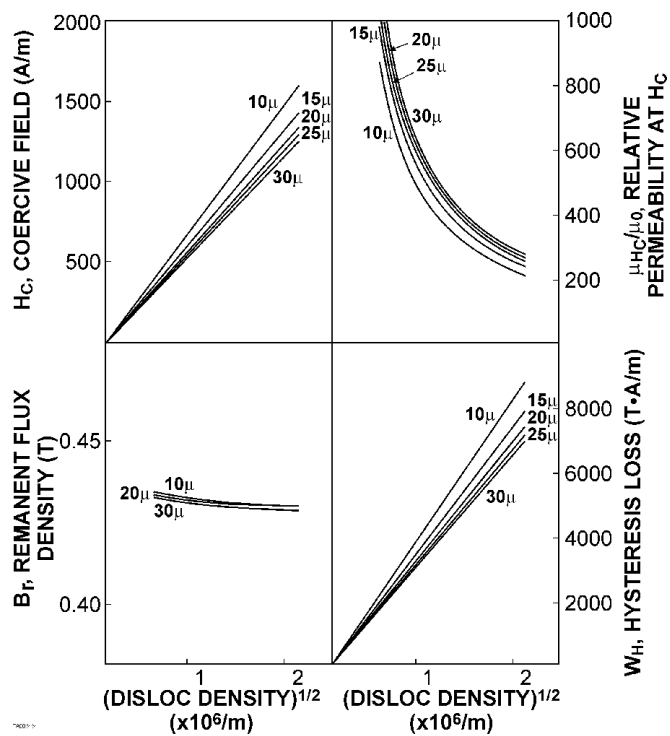


Fig. 6, M. J. Sablik, Journal of Applied Physics

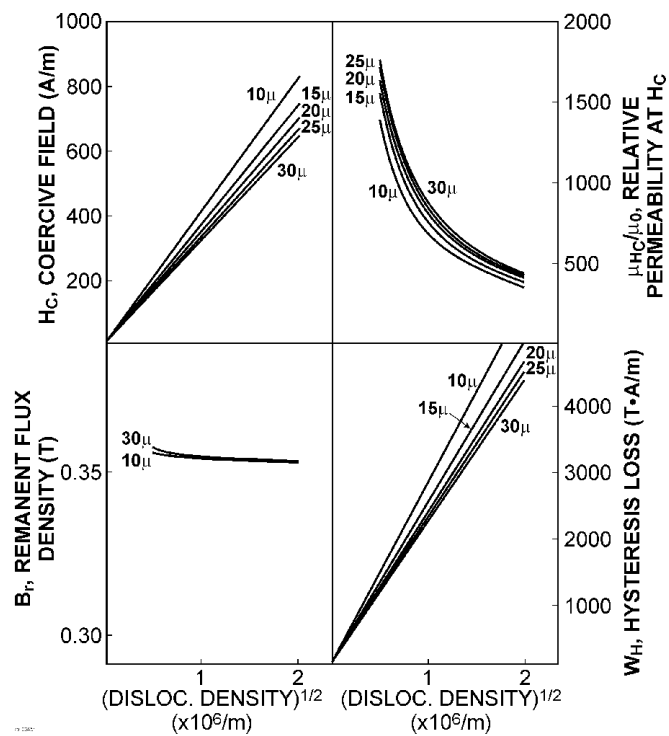


Fig. 7, M. J. Sablik, Journal of Applied Physics

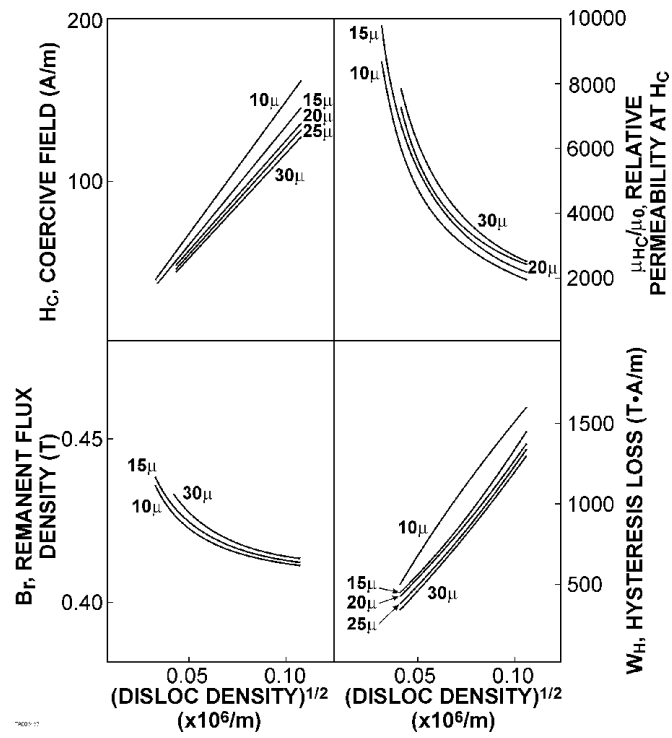


Fig. 8, M. J. Sablik, Journal of Applied Physics

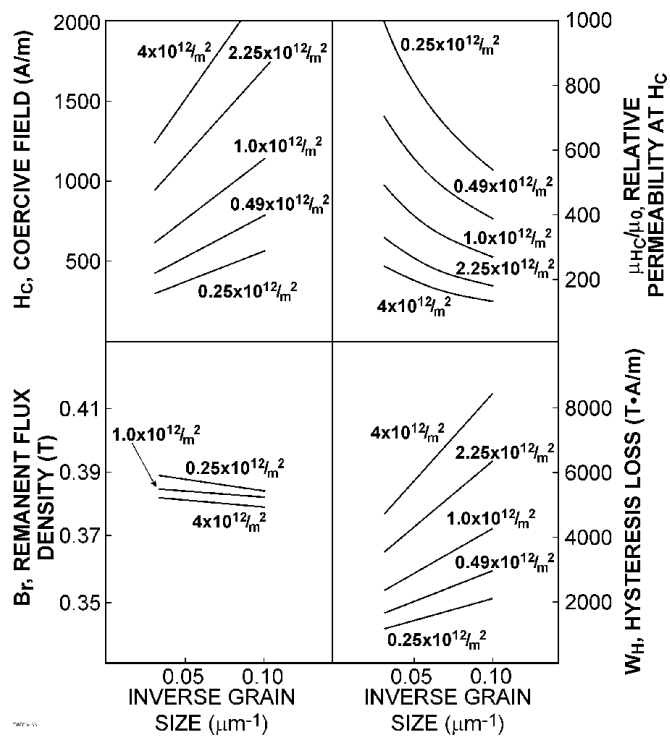


Fig. 9, M. J. Sablik, Journal of Applied Physics

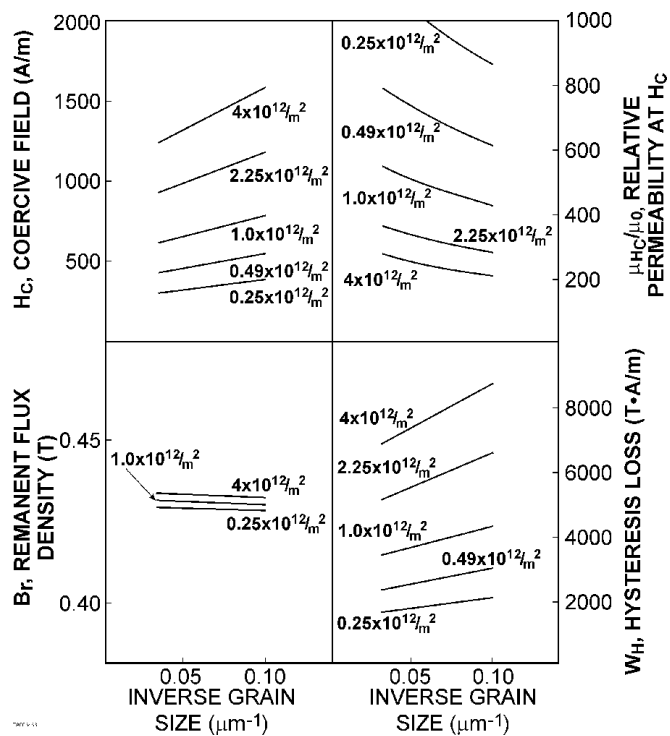


Fig. 10, M. J. Sablik, Journal of Applied Physics

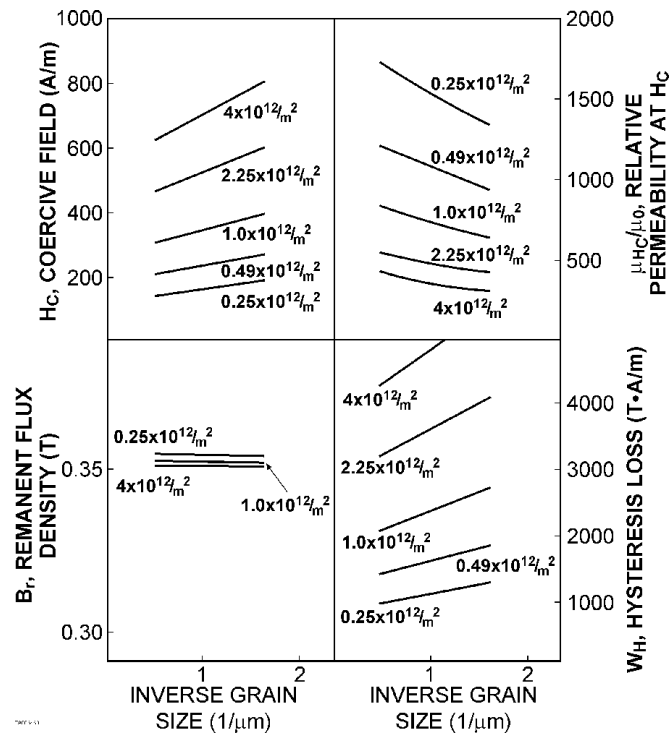


Fig. 11, M. J. Sablik, Journal of Applied Physics

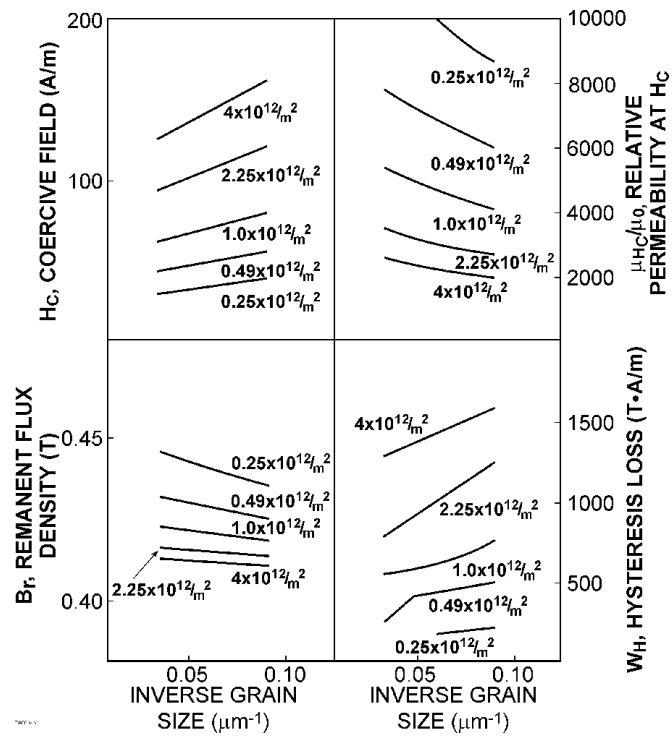


Fig. 12, M. J. Sablik, Journal of Applied Physics

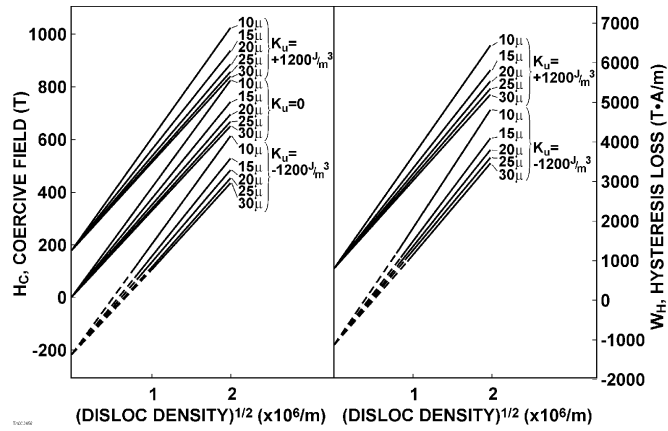


Fig. 13, M. J. Sablik, Journal of Applied Physics